Available online at www.sciencedirect.com
ScienceDirect
Thermochimica Acta 463 (2007) 44–52
thermochimica acta
www.elsevier.com/locate/tca

# Interfacial energies of *p*-dichlorobenzene–succinonitrile alloy

T. Pehlivanoğlu [a], U. Böyük [b], K. Keşlioğlu [c], A. Ülgen [d], N. Maraşlı [c,*]

[a] *Erciyes University, Institute of Science and Technology, Department of Physics, 38039 Kayseri, Turkey*
[b] *Erciyes University, Education Faculty, Department of Science Education, 38039 Kayseri, Turkey*
[c] *Erciyes University, Faculty of Arts and Sciences, Department of Physics, 38039 Kayseri, Turkey*
[d] *Erciyes University, Faculty of Arts and Sciences, Department of Chemistry, 38039 Kayseri, Turkey*

Available online 24 July 2007

**Abstract**

The commercial purity *para*-dichlorobenzene (*p*-DCB) and succinonitrile (SCN) were purified using a columnar distillation system. Thin-walled specimen cells (60–80 μm thick) were fabricated and filled with the purified materials under the vacuum. A thin liquid layer was melted and the specimen was annealed in a constant temperature gradient for an enough time to observe the equilibrated grain boundary groove shapes. The thermal conductivities of solid and liquid phases for purified *p*-DCB and *p*-DCB–2.7 mole% SCN alloy were determined with the radial heat flow and Bridgman-type growth apparatuses. From the observed grain boundary groove shapes, the Gibbs–Thomson coefficient and solid–liquid interfacial energy of solid *p*-DCB in equilibrium with *p*-DCB–SCN monotectic liquid have been determined to be $(6.1 \pm 0.6) \times 10^{-8}$ K m and $(29.2 \pm 4.4) \times 10^{-3}$ J m$^{-2}$. The grain boundary energy of *p*-DCB phase has been determined to be $(54.6 \pm 9.3) \times 10^{-3}$ J m$^{-2}$ from the observed grain boundary grooves.


*Keywords:* Organic materials; Crystal growth; Interfacial energy; Grain boundary energy; Thermal conductivity

## 1. Introduction

The solid–liquid interfacial energy, $\sigma_{SL}$, is the reversible work required to form or to extend a unit area of interface between a crystal and its coexisting liquid and plays a central role in determining the nucleation rate and growth morphology of crystals [1–3]. Thus, a quantitative knowledge of $\sigma_{SL}$ values is necessary. The measurement of $\sigma_{SL}$ in pure materials and alloys is difficult. Over the last half-century, various attempts have been made to determine the mean value of solid–liquid interfacial free energy in variety of materials [1–27]. More recently, a technique for the quantification of interfacial free energy from the solid–liquid interfacial grain boundary groove shape has been established, and measurements have been reported for several systems [7–27]. These measurements of groove shape in a thermal gradient can be used to determine the interfacial energy, independent of the grain boundary energy because the interface near the groove must everywhere satisfy

$$\Delta T_r = \left[\frac{1}{\Delta S^*}\right]\left[\left(\sigma_{SL} + \frac{d^2\sigma_{SL}}{dn_1^2}\right)\kappa_1 + \left(\sigma_{SL} + \frac{d^2\sigma_{SL}}{dn_2^2}\right)\kappa_2\right] \quad (1)$$

where $\Delta T_r$ is the curvature under cooling, $\Delta S^*$ the entropy of fusion per unit volume, $n = (n_x, n_y, n_z)$ the interface normal, $\kappa_1$ and $\kappa_2$ are the principal curvatures, and the derivatives are taken along the directions of principal curvature. Thus, the curvature under cooling is a function of curvature, interfacial free energy and the second derivative of the interfacial free energy. Eq. (1) is valid only if the interfacial free energy per unit area is equal to surface tension per unit length, $\sigma_{SL} = \gamma$. When surface energy differs from surface tension, the problem is more complicated and the precise modification of the Gibbs–Thomson equation is not yet established [4]. When the solid–liquid interfacial free energy is isotropic, Eq. (1) becomes

$$\Delta T_r = \frac{\sigma_{SL}}{\Delta S^*}\left(\frac{1}{r_1} + \frac{1}{r_2}\right) \quad (2)$$

where $r_1$ and $r_2$ are the principal radii of curvature. For the case of a planar grain boundary intersecting a planar solid–liquid

* Corresponding author. Tel.: +90 352 4374901x33114; fax: +90 352 4374933.
*E-mail address:* marasli@erciyes.edu.tr (N. Maraşlı).

0040-6031/$ – see front matter © 2007 Elsevier B.V. All rights reserved.
doi:10.1016/j.tca.2007.07.012

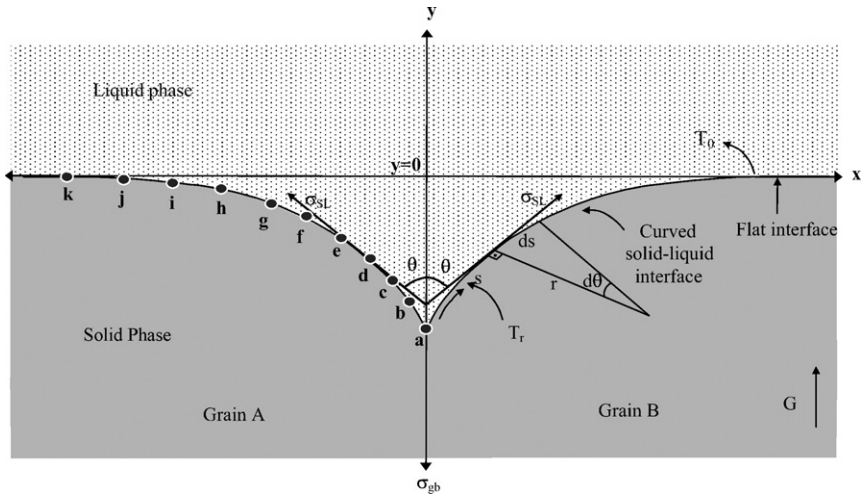


Fig. 1. Schematic illustration of an equilibrated grain boundary groove formed at a solid–liquid interface in a temperature gradient showing the definitions of $r$, $\theta$ d$\theta$, d$s$, $x$ and $y$ in Eq. (5) and the points used in determination of the Gibbs–Thomson coefficient.

interface, $r_2 = \infty$ and Eq. (2) becomes

$$\Gamma = r\Delta T_r = \frac{\sigma_{SL}}{\Delta S^*} \tag{3}$$

where $\Gamma$ is the Gibbs–Thomson coefficient. This equation is called the Gibbs–Thomson relation.

Eq. (3) may be integrated in the $y$ direction (perpendicular to the macroscopic interface) from the flat interface to a point on the cusp

$$\int_0^y \Delta T_r \, dy = \Gamma \int_0^y \frac{1}{r} \, dy \tag{4}$$

The right-hand side of Eq. (4) may be evaluated for any shape by noting that by definition d$s = r$ d$\theta$ and d$y = r\cos\theta$ d$\theta$ ($s$ and $\theta$ are shown in Fig. 1.) so that

$$\Gamma \int_0^{-y} \frac{1}{r} \, dy = -\Gamma \int_0^y \frac{1}{r} \, dy$$
$$= -\Gamma \int_{\pi/2}^{\theta} \frac{1}{r} \, r\cos\theta \, d\theta = \Gamma(1 - \sin\theta) \tag{5}$$

The left-hand side of Eq. (4) may be evaluated if $\Delta T_r$ is known as a function of $y$. Gündüz and Hunt [15] developed a finite difference model to calculate the difference in temperature between the flat interface and points on the curved interface. The finite difference analysis is described in Ref. [15]. Typical points used in the calculation of Gibbs–Thomson coefficient with Gündüz and Hunt's model is shown in Fig. 1. Thus left-hand side of Eq. (4) could then be integrated numerically using the values of $\Delta T_r$. The right-hand side of Eq. (5) is evaluated by measuring the theta value by Gündüz and Hunt's model [15,16]. The value of $\theta$ was obtained by fitting a Taylor expansion to the adjacent points on the cusp. Usually the points from **c** to **i** shown in Fig. 1 were used to obtain more reliable $\Gamma$ values with Gündüz and Hunt's model. This numerical method calculates the temperature along the interface of a measured grain boundary groove shape rather than attempting to predict the equilibrium grain boundary groove shape. If the grain boundary groove shape, the temperature gradient in the solid, $G_S$ and the ratio of thermal conductivity of the equilibrated liquid phase to solid phase, $R = K_L/K_S$ is known or measured the value of the Gibbs–Thomson coefficient is then obtained with the Gündüz and Hunt numerical method.

One of the common techniques for measuring solid–liquid interfacial free energy is the method of grain boundary grooving in a temperature gradient. In this technique, the solid–liquid interface is equilibrated with a grain boundary in a temperature gradient as shown in Fig. 1, and the mean value of solid–liquid interfacial free energy is obtained from the measurements of equilibrium shape of the groove profile. The grain boundary groove method is the most useful and powerful technique at present available for measuring the solid–liquid interface energy and can be applied to measure $\sigma_{SL}$ for multi-component systems as well as pure materials, for opaque materials as well as transparent materials, for any observed grain boundary groove shape and for any $R = K_L/K_S$ value. Over last 25 years, the equilibrated grain boundary groove shapes in variety of materials have been observed and the measurements of the solid–liquid interfacial free energies were made from observed grain boundary groove shapes [7–27].

Although *p*-DCB has a similar solidification structure to metallic materials it has not been used as an organic analog material because of some thermophysical properties of *p*-DCB such as solid–liquid interfacial energy, Gibbs–Thomson coefficient and thermal conductivity have not been determined or known. Thus the goal of the present work was to determine the thermal conductivities of solid and liquid phases, Gibbs–Thomson coefficient, solid–liquid interfacial energy and grain boundary energy for *p*-DCB–2.7 mole% SCN alloy.

## 2. Experimental procedures

### 2.1. Preparation of test materials

The experimental technique requires the preparation of thin slides containing the high-purity test material and the necessary

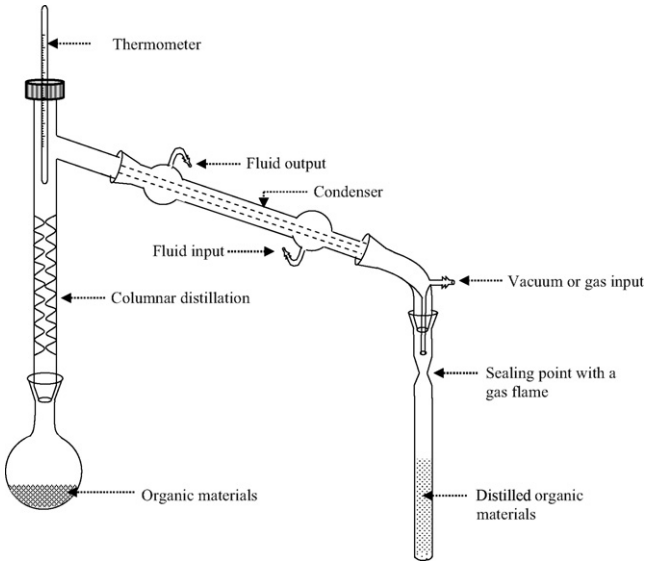


Fig. 2. The columnar distillation system, used to purify the test materials.

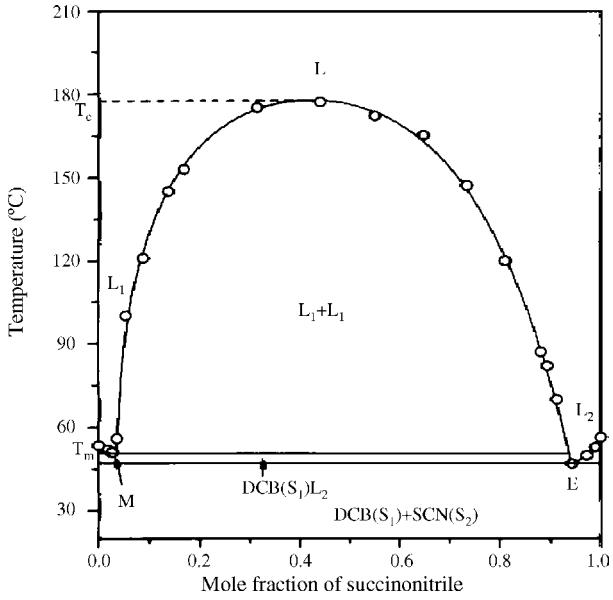


Fig. 3. Phase diagram of *p*-DCB–SCN binary alloy [35].

thermocouple assemblies. Accordingly, the preparation of specimens for purified transparent material involved three primary operations: (i) the purification of test materials by distillation, (ii) the design and assembly of the thin-slide specimen cell, and (iii) filling the specimen cell with the purified test materials under the vacuum. The relevant details regarding these procedures are given below.

Ninety-nine percent purity *p*-DCB and 99% purity SCN supplied by Merck Company was purified in quantities of approximately 100 $cm^3$ using a columnar distillation system as shown in Fig. 2. The condensation temperature for purified *p*-DCB and SCN were measured to be 383 and 393 K. The distillation was repeated four times, and the distilled materials were finally collected in a glass tube, flame-sealed under the vacuum during the distillation as shown in Fig. 2. No attempt was made to evaluate the purities of *p*-DCB and SCN. But the melting temperature of purified *p*-DCB and SCN were measured to be 326.6 and 330.8 K with a standard route under the vacuum and these values show that the purities of distilled *p*-DCB and SCN were higher than 99% purity.

The specimen cells were fabricated such that the test material was contained between two parallel ground glass plates, each being 0.15 mm in thickness, 50 mm in length, and 24 mm in width. Silicone elastomer glue was used to attach and seal the assembly on three sides with four K-type thermocouples (50 μm in diameter) fixed within the cell, distributed along the length direction with spacing of 2–3 mm. The distance between two glass plates was 60–80 μm. Before filling the cell with test material, the glue was cured for at least 24 h at room temperature to avoid any reaction between the test material and the glue.

Consider a binary monotectic system as shown in Fig. 3. Above the monotectic temperature, a binary monotectic system consists of liquid provided that the alloy composition, $C_0 < C_\alpha$, where $C_\alpha$ is the composition of the monotectic solid α phase. If the system is held in a very stable temperature gradient, the liquid droplets move to the hotter parts by temperature gradient zone melting (TGZM) and single solid α phase in equilibrium with the monotectic liquid can grow on the monotectic structure during the annealing period.

The phase diagram of the p-DCB–SCN monotectic system is shown in Fig. 3. In the present work, the alloy composition was chosen to be *p*-DCB–1 mole% SCN to observe a single solid *p*-DCB in equilibrium with the monotectic liquid (*p*-DCB–2.7 mole% SCN). DCB–1 mole% SCN alloys were prepared by the remelting of sufficient amounts of purified *p*-DCB and SCN under vacuum followed by the introduction of the material into the prepared glass cells. During this procedure, the purified materials are kept within a specialized filling chamber designed to minimize contamination from ambient air as shown in Fig. 4. Before remelting, the chamber atmosphere is evacuated and the test materials are then melted and an alloy was formed by the shaking of the filling chamber. Within the filling chamber, the open end of the test cell is immersed into the molten *p*-DCB–SCN alloy and argon gas which has a pressure of approximately 15 bar is applied to force-fill the thin slide. After filling, the slide is permitted to cool until completely solid. The specimen is removed from the chamber and the unsealed edge is sealed.

### 2.2. The temperature gradient measurement

Bayender et al. [18] utilized a temperature gradient stage to observe the equilibrated grain boundary groove shape in transparent organic materials. In the present work, a similar apparatus was employed to observe the shape of solid *p*-DCB in equilibrium with *p*-DCB–SCN monotectic liquid. The apparatus consists of hot and cold stages as shown in Fig. 5.

The hot stage is comprised of two brass plates, which are resistively heated by NiCr wires, insulated in alumina tubes and integrally threaded through the plates of the hot stage. A total of 1000 mm of heater wire, 0.5 mm in diameter was used in the hot stage, providing a maximum power of 4500 W at 220 V ac. To

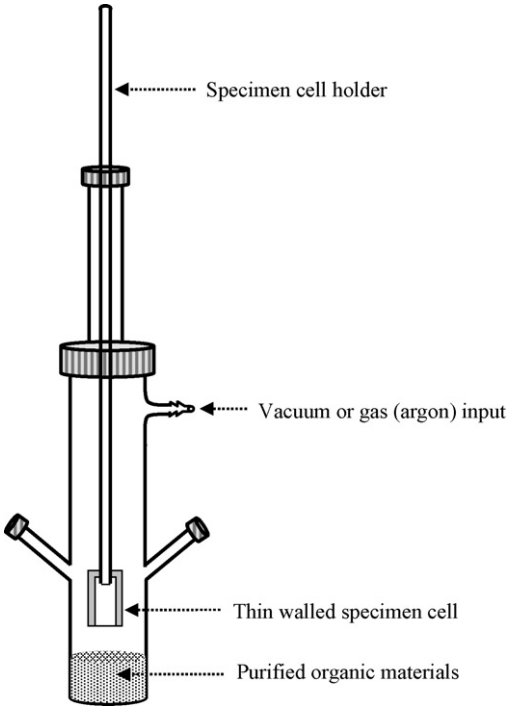


Fig. 4. Schematic illustration of the filling chamber.

maximize the thermal stability of the hot stage, a transformer was placed in the supply circuit, stepping the maximum current down to 4 A. A fully proportional thermistor-based control system was implemented, employing a control thermocouple within the hot stage. The temperature of the hot stage controlled to an accuracy of ±0.01 K with a *Eurotherm 2604* type controller.

The cold stage design is similar to that of the hot stage. However, cooling is achieved using a *PolyScience digital 9102* model heating/refrigerating circulating bath containing an aqueous ethylene glycol solution. The temperature of circulating baths was kept constant at 283 K to an accuracy of ±0.01 K.

The temperatures in the specimen were measured using three insulated K-type thermocouples with wires 50 μm thick. The end of the thermocouple wires was spark-welded. The thermocouples were calibrated by detecting the melting point of alloy.

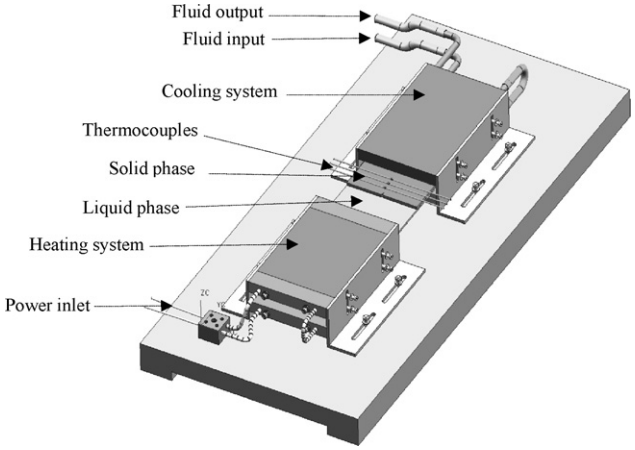


Fig. 5. Schematic illustration of the horizontal temperature gradient stage.

A thin liquid layer (2 or 3 mm thick) was melted and the specimen was held in a constant temperature gradient to observe the solid *p*-DCB in equilibrium with *p*-DCB–SCN monotectic liquid. The equilibrating time was 1 day for the *p*-DCB–1 mole% SCN alloy. When the solid–liquid interface reached equilibrium, the temperature difference between two thermocouples, $\Delta T$ was measured using a *Hewlett Packard 34401A* model digital multimeter.

The positions of the thermocouples and the equilibrated grain boundary groove shapes were then photographed with a *Honeywell CCD* digital camera placed in conjunction with an *Olympus BH2* type light optical microscope. The distance between the two thermocouples, $\Delta X$ was measured using Adobe PhotoShop 8.0 version software from the photographs of the thermocouple positions.

The temperature gradient, $G = \Delta T/\Delta X$ for the equilibrated grain boundary groove shapes was determined using the values of $\Delta T$ and $\Delta X$. The estimated error in the measurements of temperature gradient, $G$ is about 5% [20].

The coordinates of equilibrated grain boundary groove shapes were measured with an optical microscope to an accuracy of ±10 μm. The uncertainty in the measurements of equilibrated grain boundary groove coordinates was 0.1%.

### 2.3. Thermal conductivity ratio of liquid phase to solid phase

The thermal conductivity ratio of the monotectic liquid phase (*p*-DCB–2.7 mole% SCN) to solid *p*-DCB phase, $R = K_{\mathrm{L(monotectic\ liquid)}}/K_{\mathrm{S(solid\ DCB)}}$ must be known or measured to evaluate the Gibbs–Thomson coefficients with the present numerical method.

The radial heat flow method is an ideal technique for measuring the thermal conductivities in the solid. The thermal conductivities of the monotectic solid phase (*p*-DCB–2.7 mole% SCN) and solid *p*-DCB phase are needed to evaluate the value of $R = K_{\mathrm{L(monotectic\ liquid)}}/K_{\mathrm{S(solid\ DCB)}}$. In the radial heat flow method, a cylindrical sample was heated by using a single heating wire along the axis at the centre of the sample and the sample was kept in a very stable temperature gradient for a period to achieve the steady-state condition. At the steady-state condition, the temperature gradients in the cylindrical specimen is given by Fourier's law:

$$\frac{\mathrm{d}T}{\mathrm{d}r} = -\frac{Q}{AK_{\mathrm{S}}} \tag{6}$$

where $Q$ is the total input power from the centre of the specimen, $A$ the surface area of the specimen and $K_{\mathrm{S}}$ is the thermal conductivity of the solid phase. Integration of Eq. (6) gives

$$K_{\mathrm{S}} = \frac{1}{2\,\pi l} \ln\left(\frac{r_2}{r_1}\right) \frac{Q}{T_1 - T_2} \tag{7}$$

$$K_{\mathrm{S}} = a_0 \frac{Q}{T_1 - T_2} \tag{8}$$

where $a_0 = \ln(r_2/r_1)/2\pi l$ is an experimental constant, $r_1$ and $r_2$ ($r_2 > r_1$) the fixed distances from the centre axis of the spec-

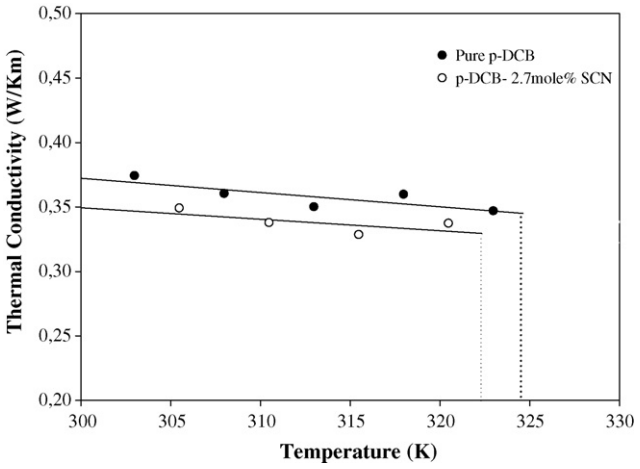


Fig. 6. Thermal conductivity of solid phase vs. time for purified *p*-DCB and *p*-DCB–2.7 mole% SCN alloy.

imen, $l$ is the length of the heating wire which is constant and $T_1$ and $T_2$ are the temperatures at the fixed positions, $r_1$ and $r_2$ from the centre axis of the specimen. Eq. (8) could be used to obtain the thermal conductivity of the solid phase by measuring the difference in temperature between the two fixed points for a given power level provided that the vertical temperature variations is minimum or zero.

The thermal conductivities of monotectic solid phase and solid *p*-DCB were measured with a radial heat flow apparatus. The details of the radial heat flow apparatus and technique are given in Refs. [15,17,28]. The sample was heated using the central heating wire in steps of 5 K up to 5 K below the monotectic melting temperature. The samples were kept at steady state for at least 2 h. At steady state the total input power and the temperatures were measured. When all desired power and temperature measurements had been completed the sample was left to cool to room temperature. The thermal conductivities of the monotectic solid phase and solid pure *p*-DCB versus temperature are shown in Fig. 6. The values of thermal conductivity of $K_{S(\text{monotectic solid})}$ and $K_{S(\text{solid } p\text{-DCB})}$ at the monotectic melting temperature were obtained to be 0.329 W/K m and 0.344 W/K m by extrapolating to the monotectic temperature, respectively and are given in Table 1.

It is not possible to measure the thermal conductivity of the liquid phase with the radial heat flow apparatus since a thick liquid layer (10 mm) is required. A layer of this size would certainly have led to convection. If the ratio of thermal conductivity of the liquid phase to solid phase is known and the thermal conductivity of the solid phase is measured at the monotectic (or melting) temperature, the thermal conductivity of the liquid phase can then be evaluated. The thermal conductivity ratio can be obtained during directional growth with a Bridgman-type growth apparatus. The heat flow away from the interface through the solid phase must balance that liquid phase plus the latent heat generated at the interface, i.e. [29]:

$$VL = K_S G_S - K_L G_L \tag{9}$$

where $V$ is the growth rate, $L$ the latent heat, $G_S$ and $G_L$ the temperature gradients in the solid and liquid, respectively and $K_S$ and $K_L$ are the thermal conductivities of solid and liquid phases, respectively. For very low velocities, $VL \ll K_S G_S$, so that the thermal conductivity ratio, $R$ is given by

$$R = \frac{K_L}{K_S} = \frac{G_S}{G_L} \tag{10}$$

A directional growth apparatus, firstly constructed by McCartney [30], was used to find out the thermal conductivity ratio, $R = K_L/K_S$. A thin-walled glass tube, 5 mm o.d., 3 mm i.d. and 180 mm total length, was used to minimize the convection in the liquid phase. Molten purified *p*-DCB and *p*-DCB–2.7 mole% SCN alloy were poured into the thin-walled glass tubes and then directionally frozen from bottom to top to ensure that the crucible was completely full. The specimen was then placed in the directional growth apparatus.

The specimen was heated to approximately 20 K over the melting temperatures of purified *p*-DCB and *p*-DCB–2.7 mole% SCN alloy. The specimen was then left to reach thermal equilibrium for at least 2 h. The temperature in the specimen was measured with an insulated K-type thermocouple. In the present work, 1.2 mm o.d. and 0.8 mm i.d. alumina tube was used to insulate the thermocouple from the melt. At the end of equilibration, the temperature in the specimen was stable to ±0.5 K for short-term period and to ±1 K for long-term period. When the specimen temperature stabilized, the directional growth was begun by turning the motor on. The cooling rate was recorded with a data logger via computer. In the present measurements, the growth rate was $8.3 \times 10^{-4}$ cm/s. When the solid–liquid interface passed the thermocouple, a change in the slope of the cooling rate for liquid and solid phases was observed. When the thermocouple reading was approximately 10–20 K below the melting temperature, the growth was stopped by turning the motor off.

The thermal conductivity ratio can be evaluated from the ratio of solid phase cooling rate to liquid phase cooling rate. The cooling rate of the liquid and solid phases is given by

$$\left(\frac{dT}{dt}\right)_L = \left(\frac{dT}{dx}\right)_L \left(\frac{dx}{dt}\right)_L = G_L V \tag{11}$$

and

$$\left(\frac{dT}{dt}\right)_S = \left(\frac{dT}{dx}\right)_S \left(\frac{dx}{dt}\right)_S = G_S V \tag{12}$$

Table 1
The thermal conductivities of solid and liquid phases and their ratios at their melting temperatures for purified *p*-DCB and *p*-DCB–SCN binary monotectic system

| Phase | Temperature (K) | $K$ (W/K m) | $R = K_L/K_S$ |
|---|---|---|---|
| Liquid (*p*-DCB–2.7 mole%SCN) | 323 | 0.237 | 0.72 |
| Solid (*p*-DCB–2.7 mole%SCN) | 323 | 0.329 | |
| Liquid (*p*-DCB–2.7 mole%SCN) | 323 | 0.237 | 0.69 |
| Solid DCB | 323 | 0.344 | |

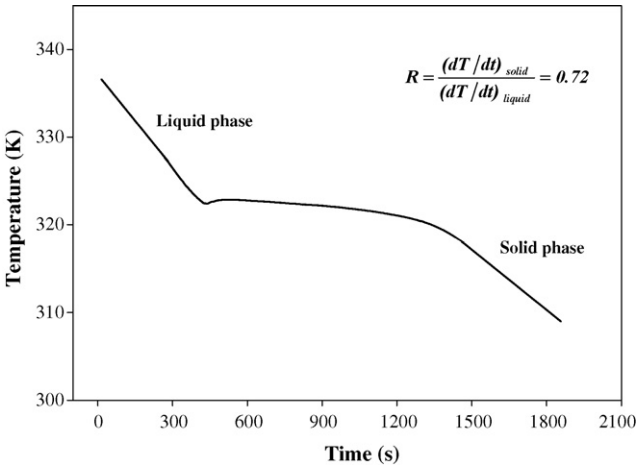


Fig. 7. Cooling rate for purified *p*-DCB–SCN monotectic alloy.

From Eq. (11)–(13), the thermal conductivity ratio can be written as

$$R = \frac{K_L}{K_S} = \frac{G_S}{G_L} = \frac{(dT/dt)_S}{(dT/dt)_L} \quad (13)$$

where $(dT/dt)_S$ and $(dT/dt)_L$ values were directly measured from the temperature versus time curves as shown in Fig. 7. The thermal conductivity ratio of liquid phase to solid phase for *p*-DCB–2.7 mole% SCN alloy was found to be 0.72, respectively, from Fig. 7 and the measured values of $K_L$ and $K_S$ for purified *p*-DCB and *p*-DCB–2.7 mole% SCN alloy are given in Table 1. Thus the thermal conductivity ratio of the monotectic liquid phase to solid *p*-DCB phase, $R = K_{L(\text{monotectic liquid})}/K_{S(\text{solid DCB})}$ is obtained to be 0.69 by using the values of $K_{L(\text{monotectic liquid})}$ and $K_{S(\text{solid DCB})}$. The estimated error in the measurements of thermal conductivity of solid and liquid phase was about 5% [28].

## 3. Results and discussion

### 3.1. The Gibbs–Thomson coefficient

If the thermal conductivity ratio of the equilibrated liquid phase to solid phase, $R = K_L/K_S$, the coordinates of the grain boundary groove shapes and the temperature gradient in the solid phase $G_S$ are known, then the Gibbs–Thomson coefficient, $\Gamma$ can be obtained using the numerical method described in detail in Ref. [15]. The experimental error in the determination of Gibbs–Thomson coefficient is the sum of experimental errors of the measurements of the temperature gradient and thermal conductivity. Thus the total error in the determination of Gibbs–Thomson coefficient was about 10%.

The Gibbs–Thomson coefficients for solid *p*-DCB in equilibrium with *p*-DCB–SCN monotectic liquid were determined by the numerical method using 10 observed grain boundary groove shapes and the results are given in Table 2. Typical grain boundary groove shapes for solid *p*-DCB in equilibrium with *p*-DCB–SCN monotectic liquid examined in the present work are shown in Fig. 8.

Table 2
The values of Gibbs–Thomson coefficient determined in present work

| Groove no. | $G_S$ ($\times 10^2$ K/m) | Gibbs–Thomson coefficient $\Gamma$ (K m) | |
|---|---|---|---|
| | | $\Gamma_{LHS} \times 10^{-8}$ | $\Gamma_{RHS} \times 10^{-8}$ |
| a | 37.6 | 6.1 | 6.2 |
| b | 45.3 | 6.2 | 6.1 |
| c | 37.0 | 6.2 | 6.1 |
| d | 36.1 | 6.2 | 6.3 |
| e | 48.0 | 6.1 | 6.0 |
| f | 47.8 | 6.1 | 6.2 |
| g | 38.5 | 6.1 | 6.2 |
| h | 37.7 | 6.2 | 6.2 |
| i | 31.8 | 6.0 | 6.1 |
| j | 45.6 | 6.0 | 6.0 |

The subscripts LHS and RHS refer to left-hand side and right-hand side of groove, respectively.

The mean value of $\Gamma$ with experimental error from Table 2 is $(6.1 \pm 0.6) \times 10^{-8}$ K m for solid *p*-DCB in equilibrium with *p*-DCB–SCN monotectic liquid.

### 3.2. The entropy of fusion per unit volume

To determine the solid–liquid interfacial free energy it is also necessary to know the entropy of fusion per unit volume and it is given by

$$\Delta S^* = \frac{\Delta H_M}{T_M} \frac{1}{V_S} \quad (14)$$

where $\Delta H_M$ is the enthalpy change of solid phase at melting temperature, $T_M$ is the melting temperature and $V_S$ is the molar volume of solid phase. Some physical property of solid *p*-DCB phase is given in Table 3. The entropy change of fusion per unit volume, $\Delta S^*$ for solid *p*-DCB was calculated to be $(4.78 \times 10^5)$ J K$^{-1}$ m$^{-3}$ as shown in Table 3. The error in the determination of entropy of fusion per unit volume is estimated to be about 5% [31].

### 3.3. The solid–liquid interfacial energy

If the values of the Gibbs–Thomson coefficient and the entropy of fusion per unit volume are measured or known, the solid–liquid interfacial energy can be obtained from Eq. (3). The experimental error in the determination of solid–liquid interfa-

Table 3
Some physical properties of the *p*-DCB–SCN monotectic alloy

| Materials | *p*-DCB–SCN |
|---|---|
| Solid phase, $C_S$ | *p*-DCB[35] |
| Liquid phase, $C_L$ | *p*-DCB–2.7 mole% SCN[35] |
| Monotectcic melting point, $T_M$ | 323.15 K [35] |
| Molecular weight of *p*-DCB, *m* | $147 \times 10^{-3}$ kg mol$^{-1}$ |
| Density of *p*-DCB, $d = m/V_S$ | $1.241 \times 10^3$ kg m$^{-3}$ |
| Molecular volume of *p*-DCB, $V_S$ | $118.45 \times 10^{-6}$ m$^3$ mol$^{-1}$[a] |
| Enthalpy change, $\Delta H_M$ | $18.3 \times 10^3$ J mol$^{-1}$ [35] |
| Entropy of fusion, $\Delta S^*$ | $4.78 \times 10^5$ J K$^{-1}$ m$^{-3}$[b] |

[a] Calculated from density definition $d = m/V_S$.
[b] Calculated from Eq. (14) using the values of $\Delta H_M$, $T_M$ and $V_S$.

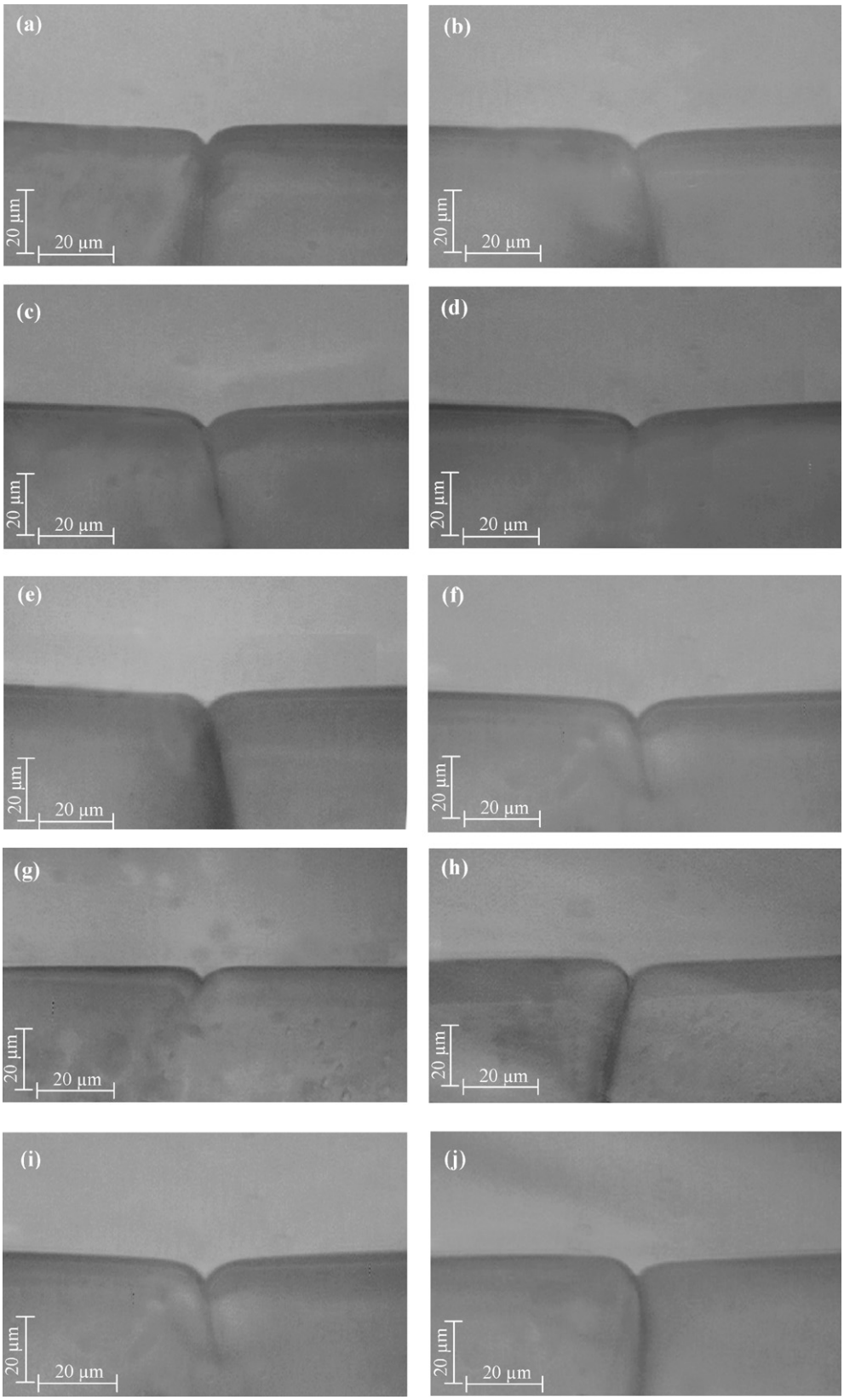


Fig. 8. Typical grain boundary groove shapes for solid *p*-DCB in equilibrium with monotectic *p*-DCB–SCN liquid.

Table 4
A Comparison of the calculated values of $\sigma_{SL}$ with the experimental values of $\sigma_{SL}$ for some organic materials

| Organic materials | $\Delta H$ (J mol$^{-1}$) | $V_S$ ($\times 10^{-6}$ m$^3$ mol$^{-1}$) | Solid–liquid interface energy, $\sigma_{SL}$ ($\times 10^{-3}$ J m$^{-2}$) | |
|---|---|---|---|---|
| | | | Calculated with Eq. (15) | Experimental |
| Succinonitrile | 3484 [32] | 76.50 | 7.9 | 7.9 [20] |
| (D) Camphor | 6865 [32] | 153.80 | 9.6 | 10.8 [22] |
| Pivalic acid | 2427 [14] | 112.70 | 4.2 | 2.7 [18], 2.8 [14] |
| Camphene | 2706 [33] | 161.80 | 3.7 | 4.4 [19] |
| Pyrene | 16,600 [34] | 159.13 | 22.8 | 21.9 [23] |
| Dichlorobenzene | 18,300 [35] | 118.45 | 30.54 | $29.2 \pm 4.4$ (present work) |

cial energy is the sum of experimental errors of Gibbs–Thomson coefficient and entropy of fusion per unit volume. Thus the total experimental error in the determination of the solid–liquid interfacial energy with the present method was about 15%. The mean value of the solid–liquid interfacial energy, $\sigma_{SL}$ for *p*-DCB in equilibrium with *p*-DCB–SCN monotectic liquid was found to be $(29.2 \pm 4.4) \times 10^{-3}$ J m$^{-2}$.

Based on nucleation experiments and classical nucleation theory, Turnbull [1] proposed an empirical relationship between the interfacial energy and melting enthalpy change to estimate the interfacial energy and it is expressed as [1]

$$\sigma_{SL} = \frac{\tau \Delta H_M}{V_S^{2/3} N_a^{1/3}} \quad (15)$$

where the coefficient $\tau$ was found to be 0.45 for metals and 0.34 for nonmetallic systems [1] and $N_a$ is the Avogadro constant. Comparisons of the calculated values of $\sigma_{SL}$ by Eq. (15) with the experimental values of $\sigma_{SL}$ for different organic materials are given in Table 4. As can be seen from Table 4, the calculated values of $\sigma_{SL}$ are in good agreement with the experimental values of $\sigma_{SL}$ except for pivalic acid.

### 3.4. The grain boundary energy

The grain boundary energy can be expressed by

$$\sigma_{gb} = 2\sigma_{SL} \cos \theta \quad (16)$$

where $\theta = (\theta_A + \theta_B)/2$ is the angle that the solid–liquid interfaces make with the *y* axis [36]. The angles, $\theta_A$ and $\theta_B$ were obtained from the cusp coordinates, *x*, *y* using a Taylor expansion for parts at the base of the groove. The mean value of grain boundary energy was then calculated from Eq. (17) using the mean value of the solid–liquid interfacial energy and the values of $\theta$. The estimated error in the determination of angles was found to be 2% from standard deviation. Thus the total experimental error in the resulting grain boundary energy is about 17%. The mean value of $\sigma_{gb}$ for solid *p*-DCB was found to be $(54.6 \pm 9.3) \times 10^{-3}$ J m$^{-2}$.

## 4. Conclusions

The commercial purity *para*-dichlorobenzene (*p*-DCB) and succinonitrile (SCN) were purified using a columnar distillation system. Thin-walled specimen cells (60–80 μm thick) were fabricated and filled with the purified materials under the vacuum. A thin liquid layer was melted and the specimen was annealed in a constant temperature gradient for an enough time to observe the equilibrated grain boundary groove shapes. The thermal conductivities of solid and liquid phases for purified *p*-DCB and *p*-DCB–2.7 mole% SCN alloy were determined with the radial heat flow and Bridgman-type growth apparatuses. From the observed grain boundary groove shapes, the Gibbs–Thomson coefficient and solid–liquid interfacial energy of solid *p*-DCB in equilibrium with *p*-DCB–SCN monotectic liquid have been determined. The grain boundary energy of solid DCB phase has also been determined from the observed grain boundary grooves.

## Acknowledgements

This project was supported by Erciyes University Scientific Research Project Unit under Contract No. FBT 06-52. The authors are grateful to Erciyes University Scientific Research Project Unit for their financial supports.

## References

[1] D. Turnbull, J. Appl. Phys. 21 (1950) 1022.
[2] D.R.H. Jones, J. Mater. Sci. 9 (1974) 1.
[3] C.L. Jackson, G.B. McKenna, J. Chem. Phys. 93 (1990) 9002.
[4] R. Trivedi, J.D. Hunt, The Mechanics of Solder Alloy Wetting and Spreading, Van Nostrand Reinhold, New York, 1993, p. 191.
[5] J.R. Morris, R.E. Napolitano, JOM 56 (4) (2004) 40.
[6] J.J. Hoyt, M. Asta, T. Haxhimali, A. Karma, R.E. Napolitano, R. Trivedi, MRS Bull. 29 (2004) 935.
[7] D.R.H. Jones, G.A. Chadwick, Phil. Mag. 22 (1970) 291.
[8] D.R.H. Jones, G.A. Chadwick, J. Cryst. Growth 11 (1971) 260.
[9] D.R.H. Jones, Phil. Mag. 27 (1978) 569.
[10] R.J. Schaefer, M.E. Glicksman, J.D. Ayers, Phil. Mag. 32 (1975) 725.
[11] S.C. Hardy, Phil. Mag. 35 (1977) 471.
[12] G.E. Nash, M.E. Glicksman, Phil. Mag. 24 (1971) 577.
[13] G.F. Bolling, W.A. Tiller, J. Appl. Phys. 31 (1960) 1345.
[14] N.B. Singh, M.E. Glicksman, J. Cryst. Growth 98 (1989) 573.
[15] M. Gündüz, J.D. Hunt, Acta Metall. 33 (1985) 1651.
[16] M. Gündüz, J.D. Hunt, Acta Metall. 37 (1989) 1839.
[17] N. Maraşlı, J.D. Hunt, Acta Mater. 44 (1996) 1085.
[18] B. Bayender, N. Maraşlı, E. Çadırlı, H. Şişman, M. Gündüz, J. Cryst. Growth 194 (1998) 119.
[19] B. Bayender, N. Maraşlı, E. Çadırlı, M. Gündüz, Mater. Sci. Eng. A 270 (1999) 343.
[20] N. Maraşlı, K. Keşlioğlu, B. Arslan, J. Cryst. Growth 247 (2003) 613.
[21] I. Stalder, J.H. Bilgram, J. Chem. Phys. 118 (2003) 798.
[22] Y. Ocak, S. Akbulut, U. Böyük, M. Erol, K. Keşlioğlu, N. Maraşlı, Scripta Mater. 55 (2006) 235.
[23] S. Akbulut, Y. Ocak, U. Böyük, M. Erol, K. Keşlioğlu, N. Maraşlı, J. Appl. Phys. 100 (2007) 123505.
[24] K. Keşlioğlu, N. Maraşlı, Mater. Sci. Eng. A 369 (2004) 294.

[25] K. Keşlioğlu, N. Maraşlı, Metall. Mater. Trans. A 35A (2004) 3665.
[26] M. Erol, N. Maraşlı, K. Keşlioğlu, M. Gündüz, Scripta Mater. 51 (2004) 131.
[27] K. Keşlioğlu, M. Erol, N. Maraşlı, M. Gündüz, J. Alloys Compd. 385 (2004) 207.
[28] M. Erol, K. Keşlioğlu, R. Şahingöz, N. Maraşlı, Metals Mater. Inter. 11 (2005) 421.
[29] D.A. Porter, K.E. Easterling, Phase Transformations in Metals and Alloys, Van Nostrnad Reinhold Co. Ltd., UK, 1991, 204.
[30] D.G. McCartney, DPhil Thesis, University of Oxford, UK, 1981, p. 85.
[31] M. Tassa, J.D. Hunt, J. Cryst. Growth 34 (1976) 38.
[32] V.T. Witusiewicz, L. Sturz, U. Hecht, S. Rex, Acta Mater. 52 (2004) 4561.
[33] E.R. Rubinstein, M.E. Glicksman, J. Cryst. Growth 112 (1991) 97.
[34] U.S. Rai, P. Pandley, J. Cryst. Growth 249 (2003) 301.
[35] R.N. Rai, U.S. Rai, Thermochim. Acta 363 (2000) 23.
[36] P. Woodruff, The Solid–Liquid Interface, Cambridge University Press, Cambridge, 1973.